jove

Histological Examination of Mitochondrial Morphology in a Parkinson's Disease Model

Dalila Ciceri[*,1], **Lierni Gregorio-Zabala**[*,1], **Xabier Llama-Pino**[1], **Begüm Kurt**[1], **Jon Olano-Bringas**[1], **Patricia Villegas-Zafra**[1], **Nora Bengoa-Vergniory**[1,2,3,4]

[1] Achucarro Basque Center for Neuroscience [2] Department of Neuroscience, University of the Basque Country (UPV/EHU) [3] Ikerbasque - Basque Foundation for Science [4] Oxford Parkinson's Disease Centre and Department of Physiology, Anatomy and Genetics, University of Oxford

[*] These authors contributed equally

Corresponding Author

Nora Bengoa-Vergniory
nora.bengoa-vergniory@dpag.ox.ac.uk

Citation

Ciceri, D., Gregorio-Zabala, L., Llama-Pino, X., Kurt, B., Olano-Bringas, J., Villegas-Zafra, P., Bengoa-Vergniory, N. Histological Examination of Mitochondrial Morphology in a Parkinson's Disease Model. *J. Vis. Exp.* (196), e65453, doi:10.3791/65453 (2023).

Date Published

June 23, 2023

DOI

10.3791/65453

URL

jove.com/video/65453

Abstract

Mitochondria play a central role in the energy metabolism of cells, and their function is especially important for neurons due to their high energy demand. Therefore, mitochondrial dysfunction is a pathological hallmark of various neurological disorders, including Parkinson's disease. The shape and organization of the mitochondrial network is highly plastic, which allows the cell to respond to environmental cues and needs, and the structure of mitochondria is also tightly linked to their health. Here, we present a protocol to study mitochondrial morphology *in situ* based on immunostaining of the mitochondrial protein VDAC1 and subsequent image analysis. This tool could be particularly useful for the study of neurodegenerative disorders because it can detect subtle differences in mitochondrial counts and shape induced by aggregates of α-synuclein, an aggregation-prone protein heavily involved in the pathology of Parkinson's disease. This method allows one to report that substantia nigra pars compacta dopaminergic neurons harboring pS129 lesions show mitochondrial fragmentation (as suggested by their reduced Aspect Ratio, AR) compared to their healthy neighboring neurons in a pre-formed fibril intracranial injection Parkinson model.

Introduction

The central nervous system has an intense demand for ATP: neurons use ATP to support ionic gradients, neurotransmitter synthesis, synaptic vesicle mobilization, release, and recycling, and to enable local protein translation and degradation. More than 95% of the ATP used by the brain is produced by the mitochondria[1]. Therefore, it is not surprising that mitochondrial dysfunction is particularly harmful to neurons. In fact, mitochondrial function impairments play an important role in several neurological diseases, including neurodegenerative conditions, such as Parkinson's Disease (PD) and Alzheimer's Disease (AD)[2,3].

Multiple genes are unequivocally linked to PD-encoding proteins that are relevant for mitochondrial function and homeostasis, such as Parkin[4,5,6], PTEN-induced kinase 1 (PINK1)[7,8] and DJ-1[9]. Further evidence for a role for mitochondrial dysfunction in PD is that treatments with inhibitors of Complex I of the mitochondrial electron transport chain (such as Rotenone and MPTP) recapitulate several aspects of PD *in vitro* and *in vivo*[10]. However, it is important to state that many pathological processes may drive neuronal loss in PD, together with mitochondrial deficits: oxidative stress, altered calcium homeostasis, failure of the ubiquitin-proteasome and of autophagy-lysosomal systems, and protein aggregation are among the most studied (reviewed in[11,12,13] and).

Mitochondria are heterogeneous in shape: in addition to individual units, they are commonly found as extended reticular and tubular networks. The structure and the cellular location of mitochondria are critical for their function[14]; in fact, mitochondrial networks are extremely dynamic, undergoing frequent processes of fission, fusion, and mitophagy in order to meet the needs of the cells and to respond to environmental cues[15,16]. In addition, the morphology of mitochondria is intimately linked to their health status. For example, in human optic atrophy, genetic mutations that reduce mitochondrial activity lead to abnormal, slender and hyperfused mitochondria[17]. On the other hand, a variety of human diseases present aberrant mitochondrial morphology, including mitochondrial fragmentation or excessive mitochondrial fusion, which have harmful effects on mitochondrial function (reviewed in[18]). In the context of PD, we and others have previously shown that abnormal mitochondrial shape correlates with dysfunction in response to α-synuclein aggregates[19]. While mitochondrial morphology has been extensively studied *in vitro* both in the context of PD and other diseases[20,21,22], protocols for the evaluation of mitochondrial morphology from *in vivo* sections are lacking. This makes the *in vivo* study of mitochondria in the context of diseases such as PD highly dependent on transgenic animals[23] or the evaluation of midbrain extracts that cannot provide cellular resolution.

Here, a protocol is presented to study the mitochondrial morphology *in situ* as an indicator of their functional status and health, based on immunostaining of the mitochondrial protein VDAC1[24] followed by image analysis in paraffin-embedded tissue sections. We also show the results of this protocol in *in vitro* and *in vivo* PD models: neuroblastoma cells overexpressing *SNCA* (Synuclein Alpha) and brain tissue from mice subjected to intracranial injection of α-synuclein Pre-Formed Fibrils (PFFs). Co-immunostaining with an antibody against α-synuclein (in cells) or phosphoSer129- α-synuclein pS129 (in mouse brains) allowed us to identify cells with aggregate protein pathology (overexpressed α-synuclein and α-synuclein fibrils, respectively) in the samples, while negative cells served as a non-pathological control within the same samples. Through this analysis and the data described here, a reduced aspect ratio was observed, indicating the fragmentation of mitochondria in cells overexpressing *SNCA* or presenting pS129 lesions.

Protocol

All procedures described in this section have been performed according to the ethical framework provided by the University of the Basque Country Reference M20/2022/212, the Government of the Basque Country, the Spanish Government, and the European Union.

1. Mitochondrial morphology analysis in *SNCA*-overexpressing SH-SY5Y cells

NOTE: Here, a brief description of the generation of the *in vitro* material for the study, which will serve as a comparison for the *in situ* obtained results, is provided. It is recommended that this type of analysis is performed before launching an *in vivo* experiment for mitochondrial morphology, as it will ensure that all appropriate imaging and analysis setups are in place.

1. To increase cellular attachment and facilitate cellular adhesion on flat optical bottom 96-well plates, add 25 µL/well of coating matrix 1:1000 in DMEM F12 by pipetting (see **Table of Materials**). Incubate the plates for 1 h at 37 °C and 5% CO_2.
2. Count SH-SY5Y using Neubauer chamber. Remove the coating matrix by pipetting, and seed 10.000 cells/well on the coated 96-well plate in 50 µL/well of DMEM F-12 supplemented with 10% FBS, 2 mM glutamine, and penicillin/streptomycin (see **Table of Materials**).
3. Incubate the cells at 37 °C and 5% $CO_2$for 24 h.
4. Prepare a mixture of 250 ng of pcDNA3.1 carrying human wild-type *SNCA*, 0.250 µL of the transfection reagent, 0.250 L of transfection adjuvant, and transfection medium up to 50 µL for each well (see **Table of Materials**). Prepare a master solution considering the total number of wells in the experiment.
5. Remove the culture medium by manual pipetting and add 50 µL/well of the solution prepared in step 1.4 by pipetting. Incubate at 37 °C, 5% CO_2.
6. h after transfection, remove the transfection medium by pipetting and add 25 µL/well of 4% paraformaldehyde (PFA) in PBS.

   CAUTION: Paraformaldehyde is a toxic fixative; use appropriate PPE.
7. Incubate for 5 min at room temperature (R.T). Remove the fixing solution by pipetting and wash once by adding 50 µL/well of PBS. Remove PBS by pipetting.
8. Pipette 25 µL/well of TBS with 0.05% Tween (TBS-T) and 10% normal donkey serum (NDS, see **Table of Materials**). Incubate for 1 h at R.T. to block any unspecific signal.
9. Prepare a solution of Rabbit-anti-α-synuclein antibody MJFR1 1:1000 together with Mouse-anti-TOMM20 antibody 1:100 in TBS-T (see **Table of Materials**) according to the number of wells to analyze.
10. Remove the blocking solution from step 1.8 by pipetting and add 25 µL/well of the mixture of primary antibodies prepared in step 1.9. Incubate overnight at 4 °C.
11. Remove the primary antibody solution and wash three times by adding and removing 50 µL/well of TBS-T by pipetting.
12. Prepare a solution of green secondary antibody anti-Mouse 1:1000 together with red secondary antibody anti-Rabbit 1:1000 in TBS-T (see **Table of Materials**) according to the number of wells to analyze.
13. After aspirating the PBS from the last wash described in step 1.11, add 25 µL/well of the secondary antibody mixture using a pipette and incubate the plate for 1 h at R.T.
14. Remove the secondary antibody solution by pipetting and add 25 µL/well of 2 g/mL DAPI in TBS-T. Incubate the plate for 5 min at R.T.

15. Remove the DAPI solution using a pipette and wash three times by adding and removing 50 µL/well of TBS-T with a pipette.

16. Pipette 80 µL/well of PBS with 0.02% sodium azide and store the plate at 4 °C.
    CAUTION: Sodium azide is toxic; use appropriate PPE.

17. Capture images using a high-content automated fluorescence microscope or equivalent confocal imaging system equipped with a 60x objective (see **Table of Materials**).

18. Perform analysis of the TOMM20 signal of single cells using Fiji following steps 3.15-3.21. Avoid any cells undergoing apoptosis, necrosis, or mitosis.
    NOTE: To do so, we exclude from the analysis the cells showing those morphological features of apoptosis, necrosis, or mitosis that are visible under the microscope, such as cell shrinkage, membrane blebbing, cell detachment, nuclear condensation, DNA fragmentation, and condensed nuclear chromatin organized into thick strands aligned in a single plane.

2. The generation of PFFs and PFF intracranial injections in mice

NOTE: The generation of injection material and the intracranial injection process are presented here. This protocol is adapted from Luk et al.[25].

1. To obtain PFFs, place a tube/flask containing 0.5 mL of α-Syn (5 mg/mL; Peptide, see **Table of Materials**) on a shaker at 37 °C and 250 r.p.m. for 7 days to induce aggregation of α-synuclein.

2. Sonicate the aggregated α-synuclein at 20% amplitude and 0.25 cycle duty until optimal fragmentation was achieved and observed by negative staining of the samples with transmission electron microscopy.

3. To prepare male and female wild-type C57Bl/6 mice (3 months old) for striatal PFF injections, administer Meloxicam/Metacam (5 mg/kg) in saline solution subcutaneously. Also administer 1 mL of the sterile saline solution *via* two 0.5 mL subcutaneous injections per animal. These treatments prevent dehydration, inflammation, and pain.

4. Induce anesthesia with 4% isoflurane and 0.7 L/min O_2 in an induction chamber. Check the depth of anesthesia by the lack of pedal response.

5. Shave the upper part of the mouse head and gently insert the animal into the frame of the stereotactic apparatus on a heat mat.

6. Maintain the anesthetic plane by providing animal inhalation anesthesia (1%-2% Isoflurane in 0.7 L/min O_2) through a face mask during the whole injection process.

7. Place the animal on the stereotactic frame. Disinfect the operating area with three rounds of alternating chlorhexidine scrub and 70% ethanol. Apply Marcaine/ Bupivacaine locally (around 100 µL) as a subcutaneous infiltration of 0.25%.

8. Perform a 0.5 cm incision of the skin to expose the skull and drill a 1 mm diameter hole into the skull to expose the brain surface, in the following coordinates from Bregma: - 0.5 mm anteroposterior, +/− 2.5 mm mediolateral.

9. Inject 1.5 L of PFFs obtained in step 2.2 by stereotactic delivery to the coordinates indicated in step 2.8 from Bregma and -2.7 mm dorsoventral (from the top brain) at a flow rate of 100 nl/min with a 32-G Hamilton syringe. Withdraw the syringe 5 min post-injection.

10. Suture (size: 4-0, 45 cm, see **Table of Materials**) the wound with three to five stitches as required, and bond each of them with 2 double knots and then a single knot. Stop anesthetic inhalation and remove the mouse from the frame.
11. Leave the mouse to recover in an appropriate recovery cage before returning it to its home cage.
12. During the following week, perform daily postoperative checks. Any animal's pain, distress, or discomfort should be dosed with Meloxicam/Metacam as indicated in step 2.3 every 24 h.
13. Three months later, inject 300 µL of 200 mg/mL sodium pentobarbital in saline solution *via* an intraperitoneal injection. Once the pain reflex is lost, make an incision (2-3 cm) on the chest and lift the ribs to expose the heart.
14. Transcardially perfuse with 10 mL of PBS and 35 mL of 4% paraformaldehyde in PBS one after the other at 5 mL/min using a 50 mL syringe connected to a 23 G butterfly needle.
15. Remove the brain and postfix in 4% PFA for an additional 24 h at 4 °C. Store it in 70% ethanol at 4 °C after PFA treatment.
16. Put the brain into appropriate plastic embedding boxes (see **Table of Materials**) and incubate in 95% ethanol for 1 h at R.T. Repeat the step in fresh 95% ethanol and incubate again for 1 h.
17. Transfer brains to 100% ethanol for 1 h at R.T. Repeat the step in fresh 100% ethanol and incubate again for 1 h.
18. Transfer brains into xylene or xylene substitute for 1 h at R.T. Repeat in fresh solution and incubate again for 1 h.
19. Remove the xylene or xylene substitute and incubate the sample in warm paraffin for 1 h. Replace the paraffin and incubate for an additional hour.
20. Mount the brain on the embedding boxes with warm paraffin and let it dry overnight. Prepare 5 µm sections using a microtome (see **Table of Materials**) and mount them on glass slides.

3. Mitochondrial morphology analysis by immunohistochemistry on paraffin-embedded brain slices from PFF-injected mice

1. Dewax the slides by dipping in xylene substitute ten times. Incubate the slides for 2 min in xylene substitute. Dip again ten times in xylene substitute.
   NOTE: This step is necessary to remove the paraffin and enable the rehydration of the samples.
2. Rehydration: repeat the procedure described in step 3.1 with the following solutions: 100% EtOH, 95% EtOH, 70% EtOH, and twice with ddH_2O in order.
3. Perform antigen retrieval and immunostaining following the steps below.
   1. Start by transferring the samples to a microwavable container with ddH_2O.
   2. Warm-up 100x citrate buffer pH 6 (see **Table of Materials**) stored at 4 °C (detergents may have precipitated) and prepare 350 mL of fresh 1x citrate buffer. Then pour the citrate buffer into a convenient plastic container with a lid.
   3. Put the slides into the citrate buffer container (CRITICAL: check that the slides are beneath the level of the buffer) and put the lid on.
      CAUTION: Ensure the lid is NOT completely closed, otherwise the container may burst in the microwave.

4. Microwave at 700 W: 4 min + 5 min rest, 1.5 min + 5 min rest. Top-up citrate buffer and microwave again 1.5 min + 5 min rest, 1.5 min + 5 min rest, 1.5 min + 5 min rest.

5. Cool down the samples in citrate buffer on ice for 20 min. Wash the sample with ddH_2O.

   NOTE: Antigen retrieval may vary according to specific antibody requirements.

4. Dry the sample slides with paper towel without touching the tissue. Draw rectangles with a pap pen (see **Table of Materials**) around the pieces of tissue.

5. Transfer all slides to a slide immune-staining box and wash a couple of times gently with TBS + 0.05 % TWEEN (TBS-T). Check TBS-T drops stay inside the pap-pen rectangles.

6. Remove TBS-T from the samples by tapping on paper towel. Add 50 µL of a blocking solution (10% NDS in TBS-T) into each rectangle (without touching the tissue) and incubate for 1 h at RT.

   NOTE: Volumes may vary according to the size of the tissue; try to ensure that: (1) the pap-penned area is similar across samples, and (2) the area is fully covered by the chosen buffer volume.

7. Remove the blocking solution from the samples by tapping a paper towel. Gently pipette 50 µL/rectangle of the following primary antibody mixture in TBS-T: anti-Tyrosine Hydroxylase 1:250 together with anti-VDAC1 1:100 and anti-pSer129 α-synuclein EP1536Y 1:2000 (see **Table of Materials**).

8. Incubate overnight at 4 °C.

9. Wash by pipetting TBS-T on the slides and remove it by tapping on paper towel. Repeat three times.

10. Add by pipetting 50 µL/rectangle of secondary antibody mixture: green secondary anti-Chicken, red secondary anti-Mouse, and far red secondary anti-Rabbit 1:1000 in TBS-T (see **Table of Materials**). Incubate at 37 °C for 1 h in the dark.

11. Wash three times with TBS-T as described in step 3.13.

12. Incubate with DAPI 2 µg/mL in TBS-T for 1 min. Remove the DAPI solution by tapping on paper towel. Wash three times with TBS-T as described in step 3.13.

13. Mount a glass coverslip on the samples using 2 drops/slide of mounting reagent (see **Table of Materials**). Press the coverslip gently to eliminate bubbles and let the samples dry for 1 h at R.T. Afterwards, store at 4 °C in the dark.

14. Image at least 50 cells in different fields using structured illumination fluorescence imaging system equipped with 60x oil objective or confocal technology.

15. Perform analysis of the VDAC1 signal of single cells using Fiji as indicated in the following steps.

    1. First, select and isolate the **region of interest (ROI)** by drawing a contour around the positive or negative cell (as appropriate) and using the "Crop" function. In order to avoid bias in ROI selection, choose it by considering the fluorescence signal of a marker unrelated to the analysis (i.e., not a mitochondrial marker).

16. Optional: if the image is excessively pixelated, use the "smooth" function to obtain a higher edge definition.

    NOTE: Should the smooth function be applied to an image, please apply it to all subsequent images.

17. Optional: use the "Convolve" function (Kernel mode, in **Process > Filters**) to reduce the background.

NOTE: This is optional and usually not necessary when using 5 m sections due to the thinner nature of the sections.

18. Activate the **shape descriptors** and **limit to threshold** options on the "Set measurement" function (ensure these are activated through the analysis).

19. In the "Adjust" menu, select the **threshold function** and adjust the threshold level. The threshold settings must be maintained for all cells of the same sample.

    1. Try to ensure adequate visualization of the mitochondrial network, as shown in the representative images of this article, while discarding background pixels.

20. Use the **Analyze particles** tool on Analyze tab. Set an appropriate size to capture the mitochondria. In this example, size: **25-Infinity**, activate: **Pixel units**, and select: **Show: Masks** commands were used to visualize the result. Fiji will calculate and display the counts, Aspect Ratio (AR), and other shape parameters in a new panel.

21. Perform statistical analysis of the data as appropriate. In this experiment, the t-test was used to analyze the difference in average Aspect Ratio (AR) and Counts calculated by Fiji between the experimental groups after normality testing with the D'Agostino and Pearson normality tests.

Representative Results

In order to ensure that the appropriate imaging and analysis conditions are in place for the *in situ* evaluation of mitochondrial morphology in tissue, an *in vitro* exploration of mitochondrial morphology in response to a known modulator of mitochondrial morphology is recommended (Section 1). As an example, SNCA was genetically overexpressed in SH-SY5Y cells to induce changes in mitochondrial morphology as previously described[26]. Other insults that could be used as a control to worsen mitochondrial morphology would be starvation or the use of mitochondrial activity inhibitors such as MPP+. Cells were transfected and stained for α-synuclein (AS) to separate *SNCA*+ (AS+) and *SNCA*- (AS-) cells. They were also stained with TOMM20[27] to visualize the mitochondrial network of cells. To make this analysis as similar as possible to that of a 5 µm tissue section, one confocal plane was analyzed as opposed to a maximum projection of multiple planes. Morphological analysis of one confocal plane of TOMM20 revealed that both the total number of mitochondria and their aspect ratio or AR (which correlates with the elongation of the organelle) were reduced in response to SNCA overexpression (**Figure 1**).

Immunostaining was performed for the mitochondrial protein VDAC1 in 5 µm paraffin-embedded mouse brain sections from animals injected with PFFs as described in the protocol section above. Substantia nigra pars compacta (SNc) dopaminergic neurons, which undergo degeneration in PD, were revealed through co-immunostaining with anti-tyrosine hydroxylase (TH) and were regionally separated from the ventral tegmental area and the substantia nigra pars lateralis. On the other hand, anti-phosphoSer129-α-synuclein (pS129) staining allowed us to discriminate cells that harbored pS129 lesions from healthy cells (pS129+ versus pS129-). SNc images of three different animals were taken, and subsequent image analysis of VDAC1 staining of TH-positive neurons revealed a reduction of both mitochondrial number counts and aspect ratio between neurons bearing pS129 lesions and neurons lacking these (**Figure 2**). These results indicate that the mitochondrial morphology of neurons harboring pS129

lesions is impaired compared to that of cells lacking pS129 lesions.

While this particular experiment shows a reduction in the AR, thereby highlighting a reduction in the elongation of mitochondria together with a reduction in global counts, which indicates a worsening of the mitochondrial morphology, the interpretation of the data should be experiment dependent. For example, a reduction in AR and counts can point to a global reduction in mitochondrial content as well as fragmentation, while a reduction in AR but an increase in global counts would point to a mitochondrial fragmentation phenotype. Therefore, it is important to interpret the data in the context of both measures.

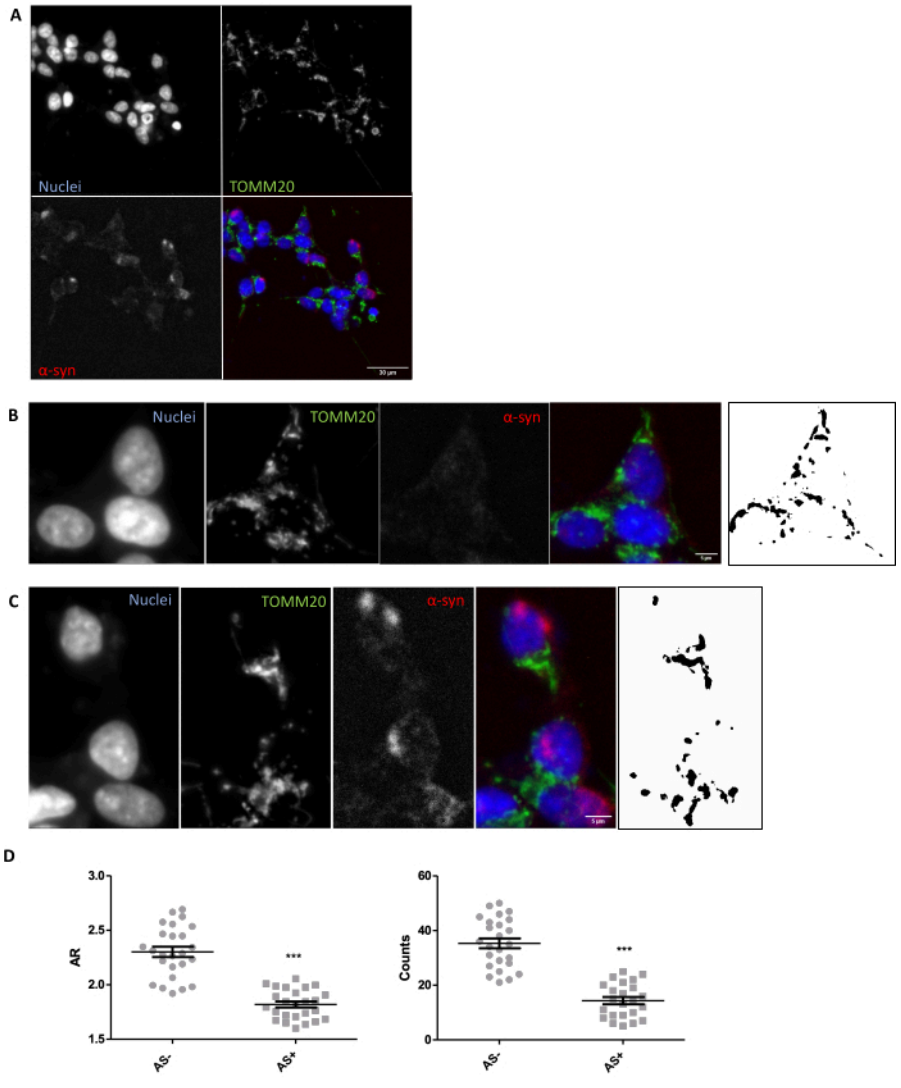

Figure 1: Mitochondrial morphology in an *SNCA*-overexpressing *in vitro* model. Co-immunostaining for TOMM20 (green), α-synuclein (AS, red), and DAPI (blue) on SNCA-overexpressing and not overexpressing (AS+ and AS-, respectively) cells (**A**). Detail of an AS- cell (B) and an AS+ cell (**C**). Black and white images in panels (**B**) and (**C**) represent

the masks of the TOMM20 signal after applying the Fiji function described in the Protocol section. This mask enables quantification of the shape of the resulting structures. Mitochondrial counts and Aspect Ratio (AR) values of AS- and AS+ cells (N = 25 cells per condition) were quantified and represented as individual values as well as average ± SEM; ***p*-value < 0.05 t-test (**D**). Normality was assessed through the D'Agostino and Pearson normality tests. Scale bars: **A**, 30 µm; **B,C**, 5 µm. Please click here to view a larger version of this figure.

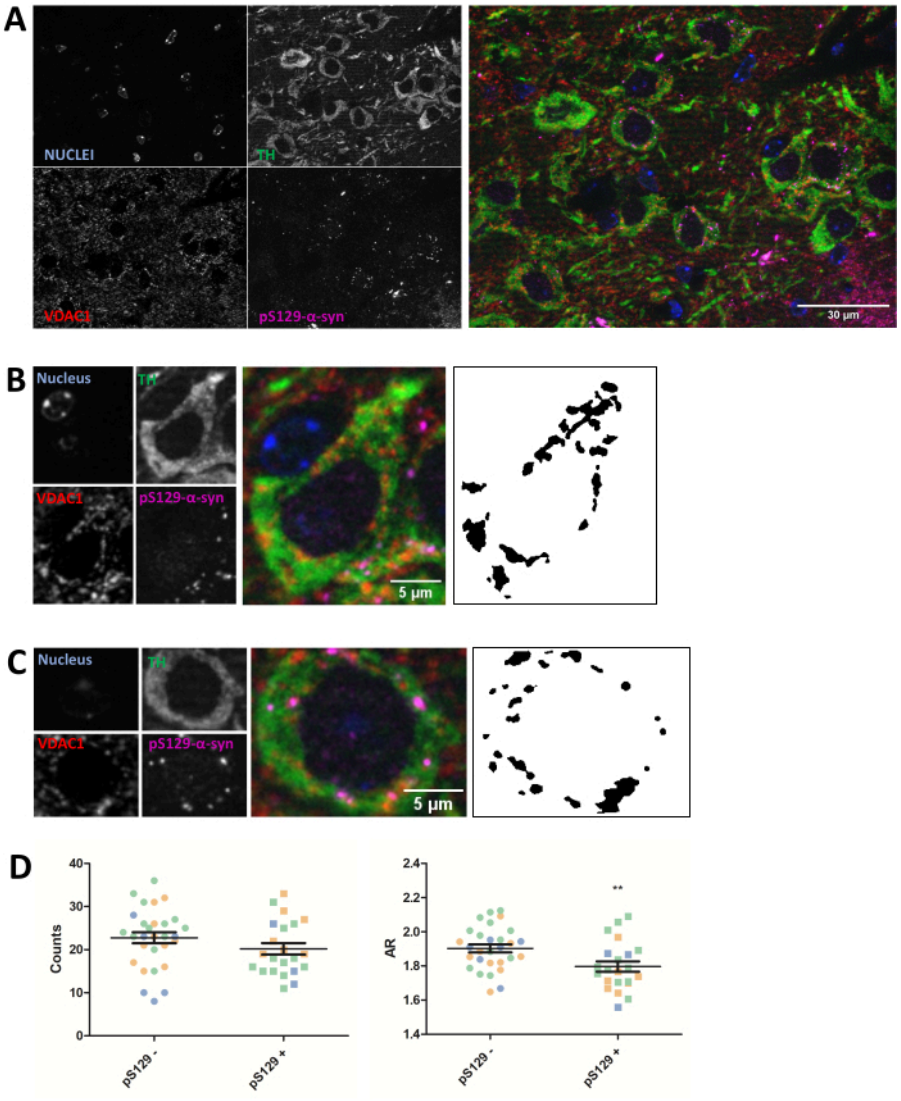

Figure 2: Mitochondrial morphology is affected in neurons harboring pS129 lesions. Co-immunostaining for TH (green), VDAC1 (red), phosphoS129-α-synuclein (magenta), and DAPI (blue) of the SNc of PFF-injected mice (**A**). The detail of a phosphoS129-α-synuclein-negative (pS129-) dopaminergic neuron (**B**) and of a phosphoS129-α-synuclein-positive (pS129+) dopaminergic neuron (**C**). Black and white images in panels (**B**) and (**C**) represent the masks of the TOMM20 signal after applying the Fiji function described in the Protocol section. This mask enables quantification of the shape of the resulting structures. Negative and positive cells were counted in samples from three different animals as illustrated by the different colors of the individual graphed values (blue, green, and orange). Mitochondrial counts and AR quantification of pS129- (N = 29) versus pS129+ (N = 22) in dopaminergic neurons were represented as average ± SEM as well as individual

cell values; **p-value < 0.05 t-test (**D**). Normality was assessed through the D'Agostino and Pearson normality tests. Scale bars: **A**, 30 µm; **B,C**, 5 µm. Please click here to view a larger version of this figure.

Discussion

Overall, this study shows that immunostaining combined with image analysis is a reliable method for analyzing mitochondrial morphology. In fact, it allows quantifying the number of mitochondria as well as some morphological parameters such as aspect ratio in both cell culture and tissue. The number of mitochondria is directly linked to the functional status of the fission and fusion mechanisms of the samples, whereas the AR value relies on the elongation of the organelle. This method may be particularly valuable for the quick evaluation of the mitochondrial abnormalities in models of PD in which altered mitochondrial morphology, dynamics and functions are well-known pathological mechanisms[28,29]. α-synuclein also plays a relevant role in PD: indeed, α-synuclein is one of the components of Lewy Bodies, the cytoplasmatic fibrillary aggregates that are used for post-mortem diagnosis of PD patients[30]. Moreover, mutations in the *SNCA* gene were found in patients with both familiar and sporadic PD (reviewed in[31]). Phosphorylation of α-synuclein at Ser129 has extensively been shown to label Lewy-Body-like pathology, which emerges after PFF insult and elicits various toxic effects[32,26].

Using the tool presented here, we were able to detect a reduction in mitochondrial number and AR values in the presence of both overexpressed and aggregated α-synuclein (cells with α-synuclein-staining and neurons bearing phosphoSer129α-synuclein-positive lesions, respectively) compared to cells lacking such lesions (α-synuclein- and phosphoS129α-synuclein-negative cells). These results agree with previous reports showing how direct α-synuclein-mitochondria interactions produce toxic effects on mitochondrial function and homeostasis in PD[26,33,34]. Indeed, it was reported that mice with α-synuclein mutations exhibit increased mitochondrial DNA damage[35] and mitophagy[36,37]. Moreover, it was described that increased α-synuclein levels promote mitochondrial fission/fragmentation, induce reactive oxygen species within mitochondria, and dysregulate mitochondrial protein expression in cell lines and mouse models overexpressing α-synuclein[26,38,39].

It is important to highlight that this tool highly depends on the antibodies used for the study; careful morphological evaluation of the antibody stain used is imperative to detect the appropriate subcellular compartment. As this technique is based on 5 µm sections and therefore requires single focal planes for the analysis of the mitochondrial structures, the absence of a phenotype will not rule out the existence of a phenotype, as it is possible that subtle differences in mitochondrial morphology may not be detected by this method.

While this work and others have previously used similar approaches to evaluate mitochondrial morphology *in vivo*[40], there is a need for a detailed protocol to be made accessible to the research community for this assessment. The significance of this study is that it is possible to apply this method to various *in vivo* disease models to assess mitochondrial morphological abnormalities and identify potential pathology, which may eventually facilitate the screening of lead compounds for the treatment of such disorders. While this analysis is currently limited to paraffin-embedded tissue, the advantage of the method is that it can be applied to any disease model after terminal tissue collection, making it a very versatile tool.

Disclosures

We wish to report no conflicts of interest.

Acknowledgments

We wish to acknowledge the funders of this study, specifically Ikerbasque, the Spanish Ministry for Science and Innovation, the Michael J Fox Foundation, IBRO, and the Achucarro Basque Center for Neuroscience.

References

1. Yang, Y., Lu, B. Mitochondrial morphogenesis, distribution, and parkinson disease. *Journal of Neuropathology and Experimental Neurology.* **68** (9), 953-963 (2009).
2. Schapira, A.H. Mitochondria in the aetiology and pathogenesis of Parkinson's disease. *The Lancet Neurology.* **7** (1), 97-109 (2008).
3. Swerdlow, R.H. Mitochondria and mitochondrial cascades in alzheimer's disease. *Journal of Alzheimer's Disease.* **62** (3), 1403-1416 (2018).
4. Hedrich, K. *et al.* Distribution, type, and origin of Parkin mutations: Review and case studies. *Movement Disorders.* **19** (10), 1146-1157 (2004).
5. Kahle, P.J., Haass, C. How does parkin ligate ubiquitin to Parkinson's disease? *EMBO reports.* **5** (7), 681-685 (2004).
6. Dawson, T.M., Dawson, V.L. The role of parkin in familial and sporadic Parkinson's disease. *Movement Disorders.* **25** (S1), S32-S39 (2010).
7. Pickrell, A.M., Youle, R.J. The Roles of PINK1, Parkin, and Mitochondrial Fidelity in Parkinson's Disease. *Neuron.* **85** (2), 257-273 (2015).
8. Zhi, L. *et al.* Loss of PINK1 causes age-dependent decrease of dopamine release and mitochondrial dysfunction. *Neurobiology of Aging.* **75**, 1-10 (2019).
9. Bonifati, V. *et al.* DJ-1(PARK7), a novel gene for autosomal recessive, early onset parkinsonism. *Neurological Sciences.* **24** (3), 159-160 (2003).
10. Chia, S.J., Tan, E.-K., Chao, Y.-X. Historical Perspective: Models of Parkinson's Disease. *International Journal of Molecular Sciences.* **21** (7), 2464 (2020).
11. Wilson, D.M., Cookson, M.R., Van Den Bosch, L., Zetterberg, H., Holtzman, D.M., Dewachter, I. Hallmarks of neurodegenerative diseases. *Cell.* **186** (4), 693-714 (2023).
12. Moore, D.J., West, A.B., Dawson, V.L., Dawson, T.M. Molecular pathophysiology of Parkinson's disease. *Annual Review of Neuroscience.* **28** (1), 57-87 (2005).
13. Olanow, C.W., Tatton, W.G. Etiology and pathogenesis of Parkinson's disease. *Annual Review of Neuroscience.* **22** (1), 123-144 (1999).
14. Nunnari, J., Suomalainen, A. Mitochondria: In sickness and in health. *Cell.* **148** (6), 1145-1159 (2012).
15. Okamoto, K., Shaw, J.M. Mitochondrial Morphology and Dynamics in Yeast and Multicellular Eukaryotes. *Annual Review of Genetics.* **39** (1), 503-536 (2005).
16. Malpartida, A.B., Williamson, M., Narendra, D.P., Wade-Martins, R., Ryan, B.J. Mitochondrial Dysfunction and Mitophagy in Parkinson's Disease: From Mechanism to Therapy. *Trends in Biochemical Sciences.* **46** (4), 329-343 (2021).
17. Zou, W. *et al.* Nanoscopic quantification of sub-mitochondrial morphology, mitophagy and mitochondrial dynamics in living cells derived from patients with

mitochondrial diseases. *Journal of Nanobiotechnology.* **19** (1), 136 (2021).

18. Navaratnarajah, T., Anand, R., Reichert, A.S., Distelmaier, F. The relevance of mitochondrial morphology for human disease. *The International Journal of Biochemistry & Cell Biology.* **134**, 105951 (2021).
19. Zambon, F. *et al.* Cellular α-synuclein pathology is associated with bioenergetic dysfunction in Parkinson's iPSC-derived dopamine neurons. *Human Molecular Genetics.* **28** (12), 2001-2013 (2019).
20. Cherubini, M., Lopez-Molina, L., Gines, S. Mitochondrial fission in Huntington's disease mouse striatum disrupts ER-mitochondria contacts leading to disturbances in Ca^{2+} efflux and Reactive Oxygen Species (ROS) homeostasis. *Neurobiology of Disease.* **136**, 104741 (2020).
21. Parihar, M.S., Parihar, A., Fujita, M., Hashimoto, M., Ghafourifar, P. Alpha-synuclein overexpression and aggregation exacerbates impairment of mitochondrial functions by augmenting oxidative stress in human neuroblastoma cells. *The International Journal of Biochemistry & Cell Biology.* **41** (10), 2015-2024 (2009).
22. Wiemerslage, L., Lee, D. Quantification of mitochondrial morphology in neurites of dopaminergic neurons using multiple parameters. *Journal of Neuroscience Methods.* **262**, 56-65 (2016).
23. Liu, Y.-T. *et al.* Mt-Keima detects PINK1-PRKN mitophagy *in vivo* with greater sensitivity than mito-QC. *Autophagy.* **17** (11), 3753-3762 (2021).
24. Shoshan-Barmatz, V., Shteinfer-Kuzmine, A., Verma, A. VDAC1 at the intersection of cell metabolism, apoptosis, and diseases. *Biomolecules.* **10** (11), 1485 (2020).
25. Luk, K.C. *et al.* Pathological α-Synuclein transmission initiates parkinson-like neurodegeneration in nontransgenic mice. *Science.* **338** (6109), 949-953 (2012).
26. Ryan, B.J. *et al.* REST protects dopaminergic neurons from mitochondrial and α-synuclein oligomer pathology in an alpha synuclein overexpressing BAC-transgenic mouse model. *The Journal of Neuroscience.* **41** (16), 3731-3746 (2021).
27. Yamamoto, H. *et al.* Dual role of the receptor Tom20 in specificity and efficiency of protein import into mitochondria. *Proceedings of the National Academy of Sciences.* **108** (1), 91-96 (2011).
28. Exner, N., Lutz, A.K., Haass, C., Winklhofer, K.F. Mitochondrial dysfunction in Parkinson's disease: molecular mechanisms and pathophysiological consequences. *The EMBO Journal.* **31** (14), 3038-3062 (2012).
29. Grünewald, A., Kumar, K.R., Sue, C.M. New insights into the complex role of mitochondria in Parkinson's disease. *Progress in Neurobiology.* **177**, 73-93 (2019).
30. Baba, M. *et al.* Aggregation of alpha-synuclein in Lewy bodies of sporadic Parkinson's disease and dementia with Lewy bodies. *The American journal of pathology.* **152** (4), 879-84 (1998).
31. Vázquez-Vélez, G.E., Zoghbi, H.Y. Parkinson's disease genetics and pathophysiology. *Annual Review of Neuroscience.* **44** (1), 87-108 (2021).
32. Mahul-Mellier, A.-L. *et al.* The process of Lewy body formation, rather than simply α-synuclein fibrillization, is one of the major drivers of neurodegeneration.

Proceedings of the National Academy of Sciences. **117** (9), 4971-4982 (2020).

33. Ganguly, U. *et al.* Interaction of α-synuclein and Parkin in iron toxicity on SH-SY5Y cells: implications in the pathogenesis of Parkinson's disease. *Biochemical Journal.* **477** (6), 1109-1122 (2020).
34. Ganjam, G.K. *et al.* Mitochondrial damage by α-synuclein causes cell death in human dopaminergic neurons. *Cell Death & Disease.* **10** (11), 865 (2019).
35. Martin, L.J. *et al.* Parkinson's Disease α-synuclein transgenic mice develop neuronal mitochondrial degeneration and cell death. *The Journal of Neuroscience.* **26** (1), 41-50 (2006).
36. Choubey, V. *et al.* Mutant A53T α-Synuclein induces neuronal death by increasing mitochondrial autophagy. *Journal of Biological Chemistry.* **286** (12), 10814-10824 (2011).
37. Chen, L., Xie, Z., Turkson, S., Zhuang, X. A53T Human α-synuclein overexpression in transgenic mice induces pervasive mitochondria macroautophagy defects preceding dopamine neuron degeneration. *The Journal of Neuroscience.* **35** (3), 890-905 (2015).
38. Kamp, F. *et al.* Inhibition of mitochondrial fusion by α-synuclein is rescued by PINK1, Parkin and DJ-1. *The EMBO Journal.* **29** (20), 3571-3589 (2010).
39. Nakamura, K. *et al.* Direct membrane association drives mitochondrial fission by the parkinson disease-associated protein α-synuclein. *Journal of Biological Chemistry.* **286** (23), 20710-20726 (2011).
40. Park, J. *et al.* Abnormal mitochondria in a non-human primate model of MPTP-induced Parkinson's disease: Drp1 and CDK5/p25 signaling. *Experimental Neurobiology.* **28** (3), 414-424 (2019).